Continuum generation from single gold nanostructures through near-field mediated intraband transitions

Michael R. Beversluis, Alexandre Bouhelier, and Lukas Novotny*
The Institute of Optics, University of Rochester, Rochester, New York 14627, USA
(Received 22 April 2003; published 30 September 2003)

A broad visible and infrared photoluminescence continuum is detected from surface-plasmon-enhanced transitions in gold nanostructures. We find that the ratio of generated infrared to visible emission is much stronger for gold nanostructures than for smooth gold films. While visible emission is well explained by interband transitions of *d*-band electrons into the conduction band and subsequent radiative recombination, the strong infrared emission cannot be accounted for by the same mechanism. We propose that the infrared emission is generated by intraband transitions mediated by the strongly confined fields near metal nanostructures (localized surface plasmons). These fields possess wave numbers that are comparable to the wave numbers of electrons in the metal, and the associated field gradients give rise to higher-order multipolar transitions. We compare photoluminescence spectra for single gold spheres, smooth and rough gold films, and sharp gold tips and demonstrate that the infrared signal is only present for surfaces with nanometer-scale roughness.

DOI: 10.1103/PhysRevB.68.115433 PACS number(s): 78.55.−m, 73.20.Mf, 68.37.−d, 07.79.Fc

I. INTRODUCTION

Visible photoluminescence from metals was first reported by Mooradian[1] in 1969. A broad emission spectrum was measured when gold and copper samples were excited with 488 or 514 nm light from an argon ion laser, or with the 300–400 nm emission bands of a high pressure mercury vapor arc lamp. Since the spectrum did not depend on the excitation wavelength, the origin was assigned to radiative recombination of holes in the *d* band with electrons in the conduction band and not to Raman scattering. This report was followed by the observation of similar continuum generation in various surface enhanced Raman scattering (SERS) experiments.[2–4] In agreement with Mooradian's luminescence model, time resolved studies showed that the continuum persisted beyond the characteristic lifetimes of Raman scattering.[5] It has been discussed that momentum conservation at a metal surface can be altered and that the observed photoluminescence could involve additional transitions.[6] Local field enhancement due to surface plasmons has been found to be a prerequisite for efficient SERS and continuum generation,[7] and a systematic study of local field enhancement in two-photon excited visible photoluminescence from rough metal films has been published by Boyd, Yu, and Shen.[8] Near-field scattering studies of rough silver films showed that the field-enhancement predominantly originates from a few locations (hot spots) where the presence of local plasmon modes leads to very large field enhancements.[9] Similar emission has been reported for gold nanoparticles[10] and, more recently, for elliptically shaped particles.[11] Recently, Varnavski *et al.* performed transient studies of visible photoluminescence using visible and ultraviolet excitation pulses,[12] and showed that photoluminescence decay is faster than 50 fs. They speculated that intraband excitations of surface plasmons might provide additional contributions to the *d*-hole relaxation rate. Alternately, the suppression of interband transitions (leaving only intraband transition) can lead to a reduction of the plasmon dephasing.[13] While visible photoluminescence from gold surfaces has been the subject of many studies, there has been no systematic investigation of *infrared* emission from gold nanostructures. In this work we show that the spectrum of the broad emission from gold nanostructures is strongly influenced by surface plasmon resonances and we demonstrate that infrared emission is not simply the red tail of the visible photoluminescence spectrum. We find that infrared emission is strongly dependent on the field confinement near nanoscale metal structures suggesting a different mechanism than for visible photoluminescence.

Because the wave vector of a visible or infrared photon is small compared to the wave vector of an electron, it is customary to neglect photon momentum when discussing electronic transitions in matter.[14] However, laser irradiated metal nanostructures give rise to very strong field confinement and thus to a broad spectrum of wave numbers at the metal surface. For instance, metal tip-enhanced fluorescence and Raman microscopy have shown that electric fields are strongly confined within 20 nm of a sharp metal tip apex.[15,16] Consequently, it may no longer be appropriate to neglect photon momentum in electronic transitions. This has already been discussed by Shalaev *et al.* in the context of two-photon excited photoemission from rough silver films.[17] Also, standard selection rules are based on the electric dipole approximation, which assumes that an optical field does not vary significantly over the length scale of an electronic system. However, the strong field confinement near metal nanostructures is accompanied by strong field gradients, implying that electric dipole selection rules might no longer be sufficient and that higher multipole orders have to be taken into account. In this article we investigate the enhancement of intraband transitions in gold by localized optical near fields. We present a detailed study of broadband continuum generation from gold nanostructures and discuss the role of higher multipole transitions and non-negligible photon momentum. We show how the surface plasmon spectral dependence affects electronic

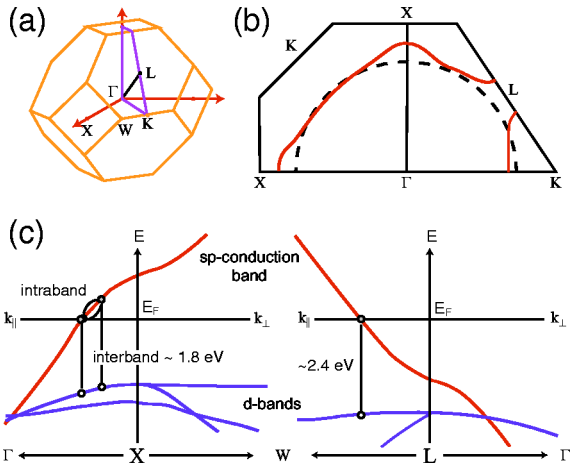

FIG. 1. (a) Symmetry points in the first Brillouin zone of gold. (b) The Fermi surface is mapped out along a path between the high-symmetry points *X* and *L* (figure from Ref. 20). Near these points, the Fermi surface is deformed from the spherical free electron surface (dashed line) due to Van Hove singularities in the density of states. (c) Regions of the band structure near *X* and *L* close to the Fermi surface. The large density of states in these regions results in interband absorption and emission processes in the visible spectrum. In contrast, infrared emission is assigned to intraband transitions, i.e., electronic states in the same conduction band.

transitions by comparing emission from smooth films with three nanostructures: isolated spheres, rough films, and sharp tips.

We have organized the remainder of this paper as follows: In Sec. II we discuss the physical processes involved in gold photoluminescence, Sec. III describes our sample preparation and experimental apparatus, Sec. IV compares the photoluminescence from smooth films with particles, and Secs. V and VI report on photoluminescence from rough films and sharp tips, respectively. These results are followed by concluding remarks.

II. OPTICAL TRANSITIONS IN GOLD

The optical properties of gold depend on both interband and intraband transitions between electronic states. The strength of these transitions is determined by the spectral overlap of two factors: (1) the energy dependent joint density of electronic states and (2) the radiation coupling efficiency defined by interfaces and nanostructure shape resonances. Following Boyd, Yu, and Shen,[8] we separate the photoluminescence generation into these two processes. The first concerns the electronic transitions within gold, and the second describes the optical coupling and enhancement specific to each sample.

Figure 1(a) shows the primary regions in the gold's first Brillouin zone in which optical transitions between the *d* bands and the conduction band occur. The Fermi surface bulges away from the free-electron sphere (dashed line) shown in Fig. 1(b) near the *X* and *L* because of van Hove singularities in the density of electronic states.[18] The large number of states causes the optical response to be dominated by the band structure in these regions, which are shown for energies within a few eV of the Fermi level in Fig. 1(c). Visible photoluminescence process begins when an electron in the *d* band is excited to an unoccupied state in the conduction band. This creates a hole in the *d* band, which after some time will recombine with an electron. Most often the recombination occurs through nonradiative mechanisms, but the hole can also radiatively recombine with electrons from the conduction band. Since the photon absorption will necessarily create *d* holes at points in the Brillouin zone where the conduction band is vacant, interband radiative relaxation is only efficient when intraband scattering processes move the holes closer to conduction band electrons at the Fermi surface. The peak energy of emitted photons is therefore strongly connected to the energy separation between *d* holes and the Fermi surface, which near *X* is roughly 1.8 eV, and near *L*, 2.4 eV. Due to these separations, visible photoluminescence is generated when the hole recombines with electrons near the Fermi surface. *Infrared* emission, on the other hand, must originate from conduction band states which are further below the Fermi surface. Due to the slope of the conduction band, the states are progressively more separated in momentum space from the region where the holes are created in the *d* band. This, along with a decrease in the density of states for these energies,[19] means that infrared photoluminescence is not efficiently generated by interband transitions.

While infrared emission is weak for smooth gold surfaces compared to visible emission, we observe very efficient infrared emission from gold nanostructures. This spectral change of the emission cannot be accounted for by interband transitions and requires an alternative explanation. Since our samples were made from pure gold, we have assumed that band structures and electron dynamics are common between them. We considered separately interband processes between occupied *d* bands to the partially filled *sp* conduction band and intraband transitions within the conduction band itself. Intraband transitions represent the free electron response of the *sp* conduction band, which is a good approximation in gold for long wavelengths. In the visible, interband processes are important, but for near-infrared wavelengths, gold behaves like a free-electron gas. The dielectric response can be described by a Drude model

$$\epsilon^f(\omega) = 1 - \frac{\omega_p^2}{\omega(\omega + i/\tau)}, \tag{1}$$

where $\omega_p = 4\pi N e^2/m_0$ is the plasma frequency for gold and τ is the electron relaxation time. From the work of Johnson and Christy,[21] $\tau = 9.3$ fs, and so in the near-infrared, $\omega \gg 1/\tau$, gold behaves similar to an ideal metal.

As indicated in Fig. 1(c), we believe that infrared emission originates from intraband transitions within the conduction band. The existence of such transitions is usually forbidden for two reason: first, a direct intraband optical transition is dipole forbidden because the initial and final electronic states have the same symmetry. Second, the states are separated by a momentum which cannot be mediated by a propagating photon. However, the evanescent fields near metal

nanostructures possess wave numbers that can be large enough to span momentum space between the initial and final states of a near-infrared intraband transition. Furthermore, the spatial confinement of the near-field results in an increase of higher-order transitions moments, such as the electric quadrupole moment, whose symmetry rules no longer prohibit intraband transitions.[22]

III. EXPERIMENTAL

A. Sample preparation

We compared the influence of nanostructure resonances (or lack thereof) on photoluminescence spectra for four samples: smooth films, isolated 100 nm spheres, rough films, and sharp tips. Smooth films were taken as a reference sample. They represent the bulk properties of gold mainly because of the lack of shape-induced resonances. Our study is then extended to well-defined resonant structures in the form of gold nanoparticles. We then investigated rough films where optical resonances are randomly distributed and are roughness dependent. Finally, optical responses of sharp metallic tips have been measured. Here, the resonances are localized at the tip apex but are strongly influenced by the shape of the tip itself.

Smooth films were formed by sputtering a 300 nm thick layer of gold onto a clean glass coverslip. To reduce the intrinsic roughness, the films were annealed at 600 °C for 12 h in a nitrogen atmosphere. The interface between the cover slip and the gold film leads to smooth films. On the other hand, rough gold films were prepared by sputtering a very thin layer of gold onto clean glass coverslips. This resulted in films with an average thickness of 10 to 20 nm, for which AFM topography images showed an average roughness of 5 to 10 nm. For purposes of comparison, some of the rough film samples were annealed at 600 °C for 12 h in a nitrogen atmosphere, while others were left unannealed. It has to be emphasized here that the annealing process of the thin layer does not influence large grain sizes but rather allows for molecularlike gold aggregates to diffuse into the sample.

Isolated gold particle samples were prepared by spin-coating a dilute particle solution onto a clean glass coverslip. The solution was taken as supplied by Ted Pella (Ted Pella, Inc., Redding, CA) which consisted of particles of an average size of 100 nm and with a variation coefficient of 8%. We used the dark-field illumination mode of our microscope to check that the particles were isolated and had not formed clusters.

Gold tips were produced by etching 99.999% pure gold wire in concentrated hydrochloric acid using the technique of Libioulle *et al.*[23] In this method, sharp gold tips are formed with short electrical pulses between the vertically submerged wire and a submerged platinum loop. The typical pulse was 30 μs in duration and 8 V in amplitude applied directly between the gold wire and the platinum loop with a repetition rate of 5 kHz. The wire is etched away until it only makes contact with the surface of the acid. The tips were then removed, rinsed with distilled deionized water, dried with nitrogen, and stored in a 10^{-2} Torr vacuum. The tips were systematically inspected and selected with a scanning electron microscope. We used tips with end radii of 5 to 30 nm. A typical gold tip is shown in Fig. 2(a).

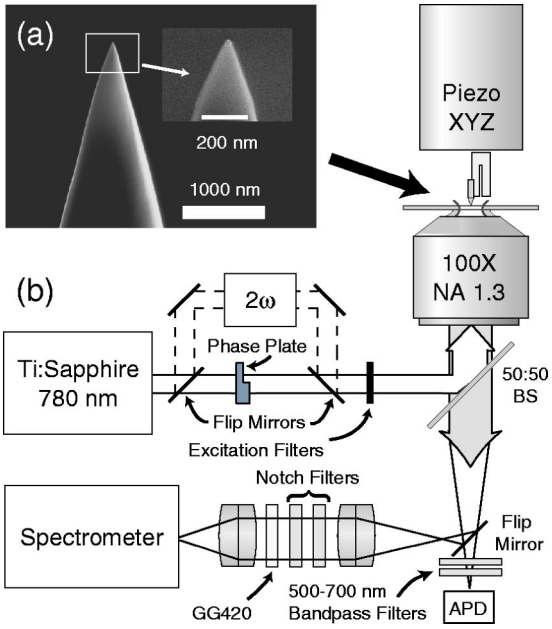

FIG. 2. (a) SEM micrographs of a 15 nm end radius gold tip. (b) Experimental setup. Pulses from a Ti:Sapphire laser (780 nm, 120 fs) are either directly sent into the microscope or first frequency doubled (2ω). The laser mode can be converted from a HG_{00} mode to a HG_{10} mode using a phase plate. The laser beam is deflected by a 50/50 beam splitter and focused by a 1.3 NA objective on the gold tip or the surfaces of other samples. Gold photoluminescence is collected by the same objective, filtered with notch and bandpass filters, and sent to a spectrometer or an avalanche photodiode (APD).

B. Experimental setup

We measured photoluminescence from the gold samples using the experimental setup shown in Fig. 2(b), which has a variety of excitation/illumination modes and possible detectors. A mode-locked Ti:sapphire laser producing 120 fs pulses at $\lambda = 780$ nm was the primary excitation source. The peak power associated with the pulse excitation allowed us to generate photoluminescence by a two-photon absorption process. Alternatively, the laser was also used in continuous wave mode or was frequency doubled using 500 μm of beta barium borate (BBO). The laser beam was linearly polarized and had a Gaussian HG_{00} intensity profile. This mode was used to excite the gold spheres and films. For some of the experiments involving the excitation of the tip, this polarization was converted to an inhomogeneously polarized HG_{10} mode. This higher-order mode is known to produce, when tightly focused, longitudinal fields oriented in direction of the propagation axis. Longitudinal fields provide the necessary polarization conditions to efficiently excite large field enhancements at the tips.[24] The conversion of the mode was obtained by placing a fused silica phase plate into the beam to introduce a relative π phase shift between two halves of the beam.[27]

Before entering the microscope, the 780 nm excitation light was filtered using a 20 nm band pass filter to remove all visible and infrared laser fluorescence. When used, the second harmonic was also filtered from laser fluorescence. The beam was spatially filtered to produce a clean transverse mode, and collimated into a 2 cm diameter beam. A 50/50 beam splitter reflected the beam into a microscope objective (1.3 NA, 100X, Plan-Fluor) focused on the sample. Alternatively, the setup allowed us to study the spectral dependence of light scattering. This is achieved by installing a dark-field illumination condenser into the microscope and by replacing the 1.3 NA objective with a 0.75 NA 40X Plan-Fluor objective. The white-light source was a quartz halogen lamp.

The film and sphere samples were scanned through the laser focus using an active feedback piezoelectric flexure stage. Tips were held above the surface using a crystal tuning-fork-based shear-force detection scheme.[28] The tips were positioned within the focus using a piezoelectric tube as sketched in Fig. 2.

The collected photoluminescence, or scattered response of our samples, was sent to either a spectrometer with a high-quantum efficiency CCD for spectral detection, or a single photon counting silicon avalanche photodiode (APD). For the spectrograph, a 4-*f* relay system was used in combination with two 780 nm notch filters. The filters removed reflected or scattered laser light with more than 12 optical densities (OD's) of attenuation. Additional filters were also used to remove light at the second-harmonic frequency. Whenever possible, measured spectra were background subtracted using the spectrum of a bare glass coverslip as reference. Integration times for measured spectra ranged between 30 and 100 s, depending on signal intensity. The measured spectral intensity has been corrected for the wavelength dependent detection efficiency of our system using the manufacturer's published values of the grating efficiency and the CCD quantum efficiency, respectively. In combination with the APD, we used dielectric band-pass filters which transmitted light between 500 and 700 nm and provided more than 12 OD of rejection outside of this band.

A simpler version of the microscope was equipped with a Hamamatsu 3680 streak camera (Hamamatsu Corporation, Bridgewater, NJ) to measure the photoluminescence transient response. A 0.13 NA objective was used to focus 780 nm femtosecond pulses onto a gold coated glass coverslip held at 45°. A 0.40 NA objective collected the photoluminescence. This system has a much larger focal spot than the previous microscope.

IV. PHOTOLUMINESCENCE FROM SMOOTH FILMS AND PARTICLES

A smooth gold interface is the simplest possible geometry for studying photoluminescence spectra. However, complications still arise from the large range of incident angles and inhomogeneous polarizations within the laser focus. For each incident ray of the laser focus, the Fresnel coefficients describing the transmission across the interface must be taken into account, and for each transmitted ray, the optical path length through the material will be different. Thus, different

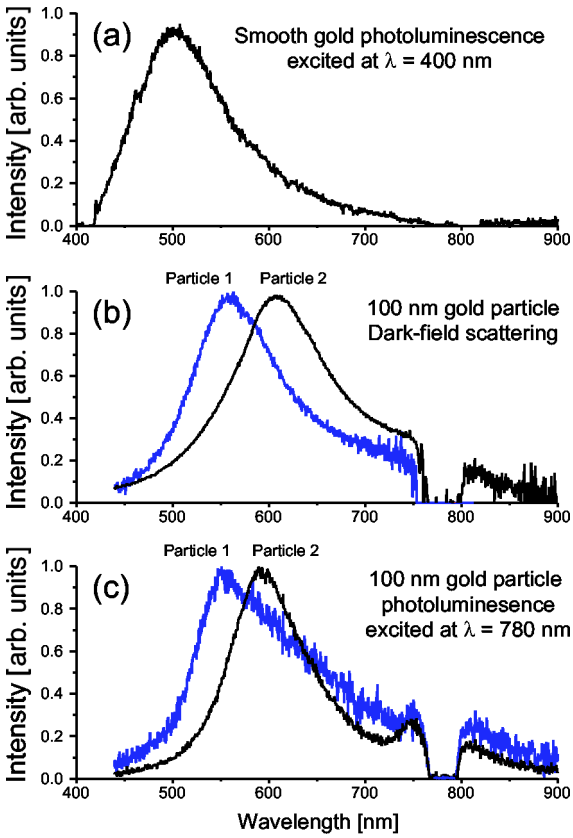

FIG. 3. (a) Gold photoluminescence from a smooth film excited by 400 nm femtosecond pulses. (b) White light dark-field scattering spectra from two gold particles (1 and 2). (c) Photoluminescence from particles 1 and 2 excited using 780 nm femtosecond pulses.

depths of the gold film will be excited at different intensities in a manner more complicated than given by a single exponential decay. Furthermore, the emission spectra from each point within the metal will depend on the emission depth and on angle. These considerations, combined with an *a priori* thermalization of the excited electronic distribution, were first calculated by Boyd for a smooth surface.[8] Apell[29] later showed that a second-order perturbative approach could describe the initial nonthermal distributions relaxation through phonons and reproduce the measured spectra.

The spectrum of interband photoluminescence from a smooth interface excited using 400 nm femtosecond pulses ($\sim$200 fs) with an average intensity of 20 μW, is shown in Fig. 3(a). Using the frequency doubled laser line allowed us to understand the spectral response of the smooth sample without additional complications due to nonlinear processes. The photon energy at $\lambda = 400$ nm is enough to excite an interband transition with a single photon. It is worth noticing that very little photoluminescence was observed by exciting the smooth film with 780 nm wavelength. The spectrum of Fig. 3(a) agrees well with the spectrum measured by Mooradian,[1] with a peak near 2.5 eV ($\sim$500 nm). This signal is attributed to photoluminescence from absorption and emission processes occurring between the uppermost *d* band and the *sp* conduction band near the *X* and *L* points in the Brillouin zone. It is important to stress that the shape of the

spectrum in Fig. 3(a) is not a result of an electronic resonance, but merely the signature of an increase of the density of states in the peak energy region.

In a next step, we measured the influence of surface plasmons on the photoluminescence spectrum. We investigated the emission of gold particles with characteristic well-defined Mie resonances.[30,31] We first measured the scattering spectrum of two individual particles using the dark-field illumination mode of our microscope. To a good approximation, the gold particle's polarizability is described by the electrostatic term in Mie's theory. This is confirmed by the normalized scattering spectra shown in Fig. 3(b). The peak wavelengths of the resonances are slightly redshifted from the static Mie value due to the relatively large particle size and the inhomogeneous surrounding dielectric function of the coverslip interface. The slight difference in the spectral peak position most likely originates from particle asymmetries. The dips in the curves centered at 780 nm are the result of the rejection filters. We then compared the scattered spectra with photoluminescence spectra by exciting the particles with 780 nm femtosecond pulses. The spectra for the same particles are shown in Fig. 3(c). In this case, the particles were excited with the 0.75 NA objective and not the 1.3 NA objective, so that a direct comparison between the scattered spectrum and the photoluminescence could be made for each particle. Subsequent measurements showed that the change in numerical aperture has no effect on the measured spectra. The average excitation power of the femtosecond pulses at the back aperture of the microscope objective was 3.4 mW, which corresponds to a peak power of approximately 1 GW/cm^2 in the center of the focus.

Comparing the four spectra shown in Figs. 3(b) and 3(c) illustrates the strong relationship between the photoluminescence and the surface plasmon peak. For both particles, the photoluminescence peak is shifted to the blue side of the surface plasmon resonance. This shift originates from the large number of available electronic states near 2.5 eV ($\sim$500 nm). The effect is not large for particle 1, whose scattering peak is at 2.25 eV ($\sim$550 nm), but for particle 2, the shift of the photoluminescence peak away from the surface plasmon peak is over 20 nm towards the blue. Since both the smooth film and particles are macroscopic polycrystals, they have the same bulk electronic properties, and the differences in the photoluminescence spectra must be due to the addition of the sphere surface plasmon resonance. It is worth noticing, that the intraband contributions, i.e., the infrared part of the spectra, are much weaker than the visible photoluminescence.

V. PHOTOLUMINESCENCE FROM ROUGH GOLD FILMS

Extensive research has gone into understanding how a nanoparticle shape is related to the magnitude of the local field enhancement produced on its surface. In single molecule SERS experiments, enhancement factors as large as 10^{14} have been observed.[32,33] Brus and co-workers have observed that large SERS enhancements are often accompanied by strong continuum generation.[34] It has also been reported that two-photon excited visible interband photoluminescence

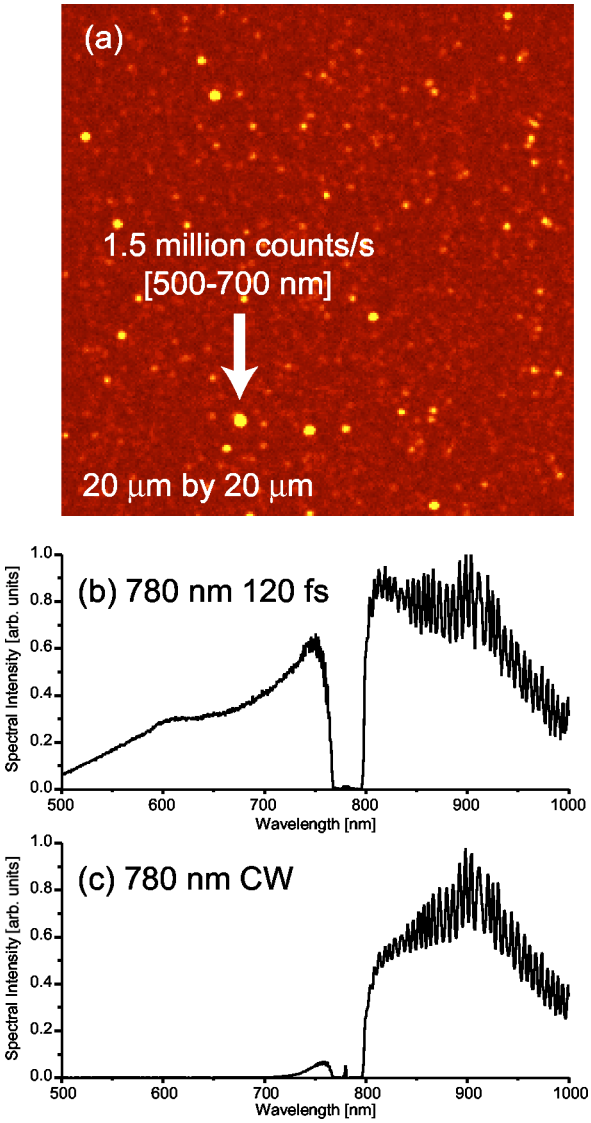

FIG. 4. (a) Visible photoluminescence from a rough gold film excited by two-photon absorption. Image size: 20×20 μm^2, $\lambda_{ex}=780$ nm. Spectra were recorded at the point indicated by the arrow in (a). Two-photon excitation was used in (b) and CW excitation in (c).

is strongly enhanced at rough films.[8] By scanning the rough film through the focus of our objective, we can identify locations of enhanced photoluminescence. A two-dimensional map of the surface optical response is reconstructed by recording the visible photoluminescence yield for each sample position. Such a map is shown in Fig. 4(a). Hot spots of localized field enhancement, which originate from isolated hemispheroidal structures or from constructive interference of multiple nanostructures, dominate the total emission intensity. The peak intensity of the 780 nm femtosecond pulses was 100 MW/cm^{-2}, but the visible photoluminescence yield at the point indicated by the arrow is a thousand times larger than what was produced previously by the isolated spheres. Figure 4(b) shows the photoluminescence spectrum at the location indicated by the arrow. While the visible photoluminescence yield at such points has been studied before, the

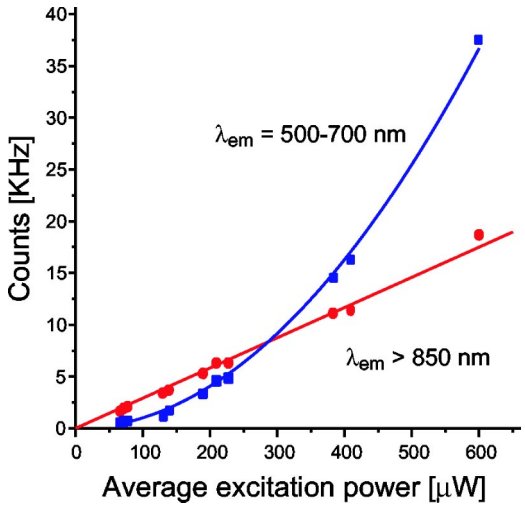

FIG. 5. Intensity dependencies of visible and infrared photoluminescence originating from a rough gold film excited at $\lambda = 780$ nm. Visible photoluminescence (500 nm $< \lambda <$ 700 nm) shows a quadratic dependence, while infrared photoluminescence ($\lambda > 850$ nm) has a linear dependence.

strong infrared signal associated with the photoluminescence has not been reported so far. A very broad infrared spectrum, that extends beyond the laser wavelength, has appeared for the rough film which was not present for single particles. The signal is constant in time and stable for more than 5 h. The infrared part appears for both femtosecond pulsed and continuous wave (cw) excitation, as shown in Fig. 4(c). As shown in Fig. 4(b), heating of the electron gas by the femtosecond pulses gives rise to additional Stokes and anti-Stokes signals near the laser wavelength. However, beyond 900 nm, the signals are identical for both pulsed and cw laser excitation, indicating a strong electronic state dependence for the signal. It should be mentioned that the fine modulation of the measured infrared spectra is caused by an etalon effect in the back illuminated CCD.

Our spectral measurements suggest that the infrared photoluminescence originates from a different mechanism than the visible photoluminescence. This difference is emphasized by the fact that the yields of visible and infrared photoluminescence do not have the same dependence on excitation intensity. As shown in Fig. 5, the spectra measured between 500 and 700 nm has a quadratic dependence when excited at $\lambda = 780$ nm. This nonlinear behavior is expected from the two-photon absorption process responsible for the visible photoluminescence. On the other hand, the infrared part, measured above 850 nm, depends linearly on the excitation intensity. This difference strongly indicates an intraband process, since a *d* hole cannot be created through a single-photon absorption at 780 nm.

We find that the enhanced infrared signal persists whenever there is surface roughness, including samples made from metal sphere clusters. For rough films and particle aggregates, annealing in a nitrogen atmosphere at 200 °C for 18 h, still resulted in hot spots with strong infrared signals. Increasing the annealing temperature to 600 °C did not remove these photoluminescence spots. Notice that similar temperatures were used for the growth of smooth gold films which show no infrared luminescence. The difference here is that the initial film thickness is only ≈ 10 nm as opposed to 300 nm used for the smooth films.

The fact that the infrared emission appeared from both annealed and unannealed rough gold films indicates that the signal is intrinsic to the bulk material and is not due to clusters of a few gold atoms. It is known that in gold clusters electronic states are localized and are molecularlike in nature. Luminescence generated by optical transitions from excited states of these clusters can span the near infrared regions.[36] However, once the cluster grows beyond a threshold of a few hundred atoms, the particle electronic states become essentially those of the bulk crystal band structure.[37] Therefore, since the electronic states are bulklike, we attribute the origin of the strong infrared signal to *intraband* transitions within the conduction band as indicated in Fig. 1(c).

Infrared emission due to intraband transitions is a weak process in bulk gold samples for the following reasons: first, the dispersion of the conduction band is large [see Fig. 1(c)], and a photon momentum cannot span the distance in *k* space between the initial and final electronic states. Second, these states both lie in the conduction band, and transitions between them are dipole forbidden due to symmetry. However, these restrictions do not apply for rough gold films and for other gold nanostructures. The characteristic wave numbers associated with strongly confined fields are much larger than the wave number of a freely propagating photon, and since the fields are no longer uniform across the dimensions of the electronic system, higher-order multipolar transitions are possible.

To better understand the origin of large wave numbers let us consider the evanescent waves confined to a particular nanostructure. Along the surface boundary, the electric field can be decomposed into an angular spectrum of plane waves and evanescent waves indexed by their wave vector **k**. The wave vector can be decomposed into components that are perpendicular and parallel to the metal surface, that is, $k_\perp$ and $k_\parallel$, and can be written as

$$k = \sqrt{k_\perp^2 + k_\parallel^2} = \frac{\omega}{c}.$$

Evanescent fields arise when $k_\perp$ becomes imaginary, and while the total wave vector magnitude is still equal to the far field value, the independent projections $k_\perp$ and $k_\parallel$ can be much larger

$$|k_\perp|, \ |k_\parallel| \gg k.$$

The largest wave number present in the near field is characterized by the inverse length of the typical distance *d* over which the field varies, i.e., $k_\parallel \approx \pi/d$. For rough metal films and for nanostructures such as a sharp gold tip, *d* can be a few nanometers. Our sputtered rough gold film has an average roughness of 5 nm which yields $k_\parallel \approx \pi/5\text{nm} \approx 10^7$ cm^{-1}. On the other hand, the Fermi wave number has a value of approximately 10^8 cm^{-1} in gold, corresponding to a length comparable to the crystal lattice constant. Taking a

simple parabolic dependence for the conduction band dispersion yields a change of wave number between the Fermi surface and an excited state of 1.6 eV above the Fermi surface of roughly $\Delta k \approx 10^7$ cm^{-1}. Therefore $k_\parallel$ is of the same magnitude as Δk, and consequently, in the near field, direct promotion of electrons to different energies within the conduction band is possible. Furthermore, the spatial confinement of the near-field results in strong field gradients and thus in an increase of the electric quadrupole moment, whose symmetry rules no longer prohibit intraband transitions.[22]

While intraband transitions should be possible within the optical near-field of a surface, the energy must be coupled to the far field for any radiation to be detected. This coupling can be mediated by the excitation of localized surface plasmons, i.e., radiatively decaying eigenmodes of the particular gold nanostructure. Localized surface plasmons couple near fields with large wave numbers to propagating radiation ($k = \omega/c$). For instance, in the one-dimensional case of a planar material interface, a surface plasmon can be coupled to far field radiation by use of a diffraction grating which compensates the momentum difference between the surface plasmon and far field radiation. It is not so simple to define the dispersion relation for a three dimensional nanostructure, but at each point along its surface the effect is similar.

Surface plasmon resonances in random media are more complicated than those of an isolated sphere, and are generally modeled by taking an ensemble average of many individual hemispheroidal bosses over an appropriate distribution of shapes and sizes.[35] It is often assumed that the spheroids do not interact with each other, although interactions can be accounted for by assuming a self-affine spatial distribution and calculating the resulting polarizability.[9] The simpler calculation has been applied to the enhancement of visible photoluminescence from various metals with a good agreement between theoretical and measured spectra.[8] Fundamental to this result is the shape resonance of an elliptical particle. In the nonretarded limit, the polarizability is given by

$$\alpha(\omega) = V \frac{\epsilon(\omega) - \epsilon_m(\omega)}{\epsilon_m(\omega) + L[\epsilon(\omega) - \epsilon_m(\omega)]}, \tag{2}$$

where V is the particle volume and ϵ and ϵ_m are the respective particle and surrounding medium dielectric functions. L is a factor which ranges between 0 and 1 depending on the particle aspect ratio and orientation to the incident electric field. L approaches 0 for fields polarized along the length of a needlelike particle.[35]

This has two important consequences: first, the plasmon resonance condition, given by the pole of Eq. (2), depends on L,

$$\epsilon = \epsilon' + i\epsilon'' \approx \epsilon_m \left(1 - \frac{1}{L}\right). \tag{3}$$

Since ϵ' becomes more and more negative in the infrared, as the particle aspect ratio increases and $1/L$ becomes large, the resonance peak must shift to longer wavelengths. The equality is approximate because of the imaginary part of the denominator in Eq. (2), which is related to the imaginary component of the dielectric function ϵ''. This leads to the second geometric factor consequence: the plasmon damping of an elliptical particle depends on its aspect ratio. Taking the imaginary part of Eq. (2) gives

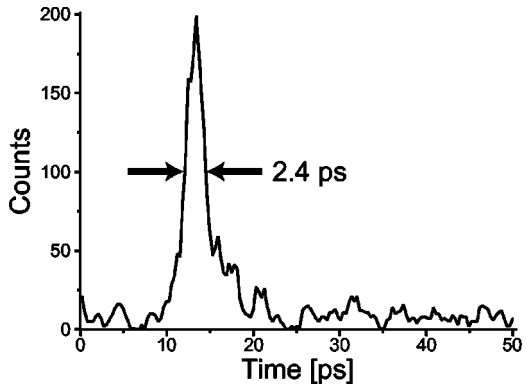

FIG. 6. Infrared ($\lambda > 830$ nm) photoluminescence transient excited at $\lambda = 780$ nm from a rough gold film measured with a streak camera. 2.4 ps reflects the instrument response function, indicating that the total relaxation lifetime of gold is shorter than 2.4 ps.

$$\mathrm{Im}(\alpha) \propto \epsilon''[\epsilon_m + L(2\epsilon' + \epsilon_m)], \tag{4}$$

where the surrounding medium dielectric is taken to be purely real. As L approaches zero, the resonance quality will increase as long as the wavelength dependence of ϵ'' does not cause it to simultaneously grow too quickly. As a consequence, rough gold films are able to support localized infrared surface plasmons. Thus, we argue that intraband emission in gold nanostructures is a three step process: (1) Local field enhancement creates optical fields with large wave numbers near the surface, (2) these large wave numbers carry enough momentum to allow direct intraband transitions within the conduction band, and (3) these transitions couple to plasmon eigenmodes of the structure and hence radiatively decay into the far field. Between the near-field and far field, the shift in the optical wave number must be mediated by a plasmon.

In order to observe photoluminescence, it is important that the radiative relaxation rate is comparable to or faster than other nonradiative relaxation rates. While Fermi-liquid theory underestimates the electron and hole lifetimes in gold,[38,39] it is still true that the higher an electron is excited above the Fermi surface, the faster the scattering channels will act to return it to thermal equilibrium.[40] The main contributions to the total decay rate are the electron-electron scattering rate (10–100 fs) and the electron-phonon scattering rate (100–1000 fs). In order for the intraband radiation to have any significant appearance, it must be nearly as fast.

We measured the transient decay of the infrared photoluminescence from gold films using a streak camera. The sample was excited using 780 nm 120 fs pulses, with a peak intensity of 200 MW/cm^2 in the focus. Only near-infrared wavelengths larger than 850 nm were detected. This wavelength range excludes the spectral components which differ between the femtosecond excited spectra and the cw spectra. The infrared photoluminescence signal resulted in the instru-

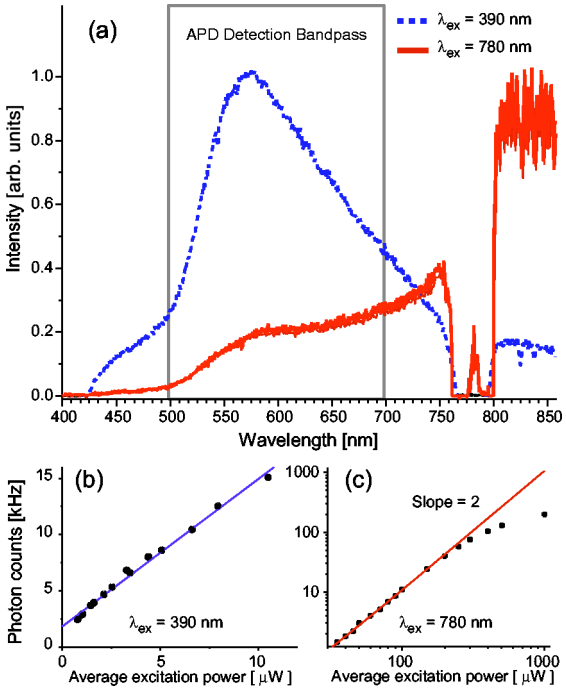

FIG. 7. (a) One- and two-photon excited emission spectra from sharp gold tips illuminated in the configuration shown in Fig. 2. The detection range of the APD is indicated by the shaded box. (b) The APD signal dependence for $\lambda = 390$ nm excitation, shown with a linear curve fit. (c) The APD signal dependence for $\lambda = 780$ nm excitation, with a quadratic curve fitted at lower intensities.

ment response function, which measured at 780 nm, was 2.3 ps full width at half maximum as shown in Fig. 6.

Measurements of the transient response of the visible photoluminescence yielded slightly longer widths of 5 ps, but due to a change in the leading slope of the transient, this seems to be a chromatic artifact of the camera. Although we believe that the intraband and interband radiative decay rates are different, this was not resolvable with our measurements. In any case, it is clear that the radiative recombination rate is competitive with nonradiative decay channels. This is reasonable considering that the energy is coupled out through the fast surface plasmon decay rate, which from the spectral width of individual nanoparticles is of the order of 2–20 fs.[13]

VI. PHOTOLUMINESCENCE FROM SHARP GOLD TIPS

While every rough gold film yields visible and infrared emission, the randomness of the surface makes it difficult to determine the size range which is critical for the efficient generation of the infrared signal. In order to gain more information about the size dependence, we investigated the photoluminescence of well characterized sharp gold tips. This allows us to study the influence of the nanostructure size, shape, and orientation on the signal enhancement. A typical spectrum emitted form a gold tip is shown in Fig. 7(a) for two laser wavelengths. The tip was placed in the focal region of the objective and adjusted to maximize the photoluminescence response. Similarly to the rough film, a white-light continuum spans the visible and extends into the near-

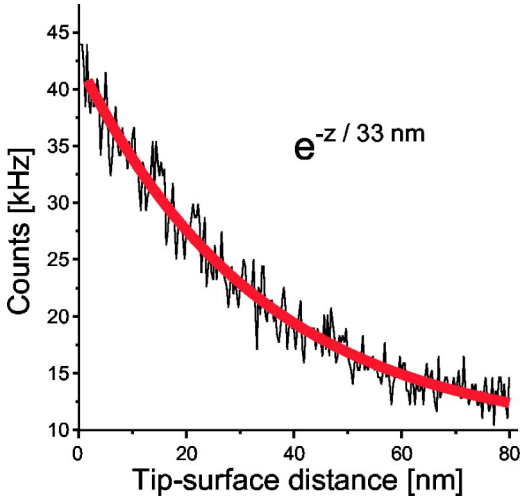

FIG. 8. Dependence of visible photoluminescence from a gold tip on the separation between tip and glass substrate. The data is fitted with a single exponential function with a decay length of 33 nm.

infrared region. The main difference between photoluminescence excited by one or two-photon absorption lies in the different cross sections of these processes. We analyzed the dependence of the visible photoluminescence signal as a function of the average excitation power and laser energy. The trends are shown in Figs. 7(b) and 7(c).

When pumped at 390 nm, the 500–700 nm emission region [shaded box in Fig. 7(a)] has a linear power dependence, indicating a one-photon excitation process. However, when pumped with 780 nm femtosecond pulses, the visible photoluminescence shows a quadratic dependence for low average intensities. This nonlinear response is consistent with a two-photon excitation process. At higher pump powers a saturation is observed. We believe that this is the result of a bleach of the *d*-band electrons. Although the total number of electrons is very large, the number of electrons laying in this narrow energy range and situated within the small excitation region near the tip apex is much less. Similarly to the rough film, the infrared region above 850 nm depends linearly on the 780 nm pump intensity (data not shown). This dependence, along with the spectral similarity of the infrared signal, which for a given tip can extend continuously to wavelengths longer than 1 micron, leads us to conclude that the infrared signal is of the same origin as the signal seen for the rough films. This is despite the very different preparation techniques between the films and tips.

An immediate advantage of the tip configuration is that the photoluminescence originates from a single well-defined source near the tip apex. The near-field nature of the photoluminescence enhancement is revealed by measuring the evanescent decay of the photoluminescence away from the tip, shown in Fig. 8. The experimental data can be fitted by a single exponential decay with a characteristic length of 33 nm. The decay length is consistent with the size of the tip and with tip-sample approach curves for near-field Raman and fluorescence studies.[15,16]

Enhanced fields near metal nanostructures are the result of

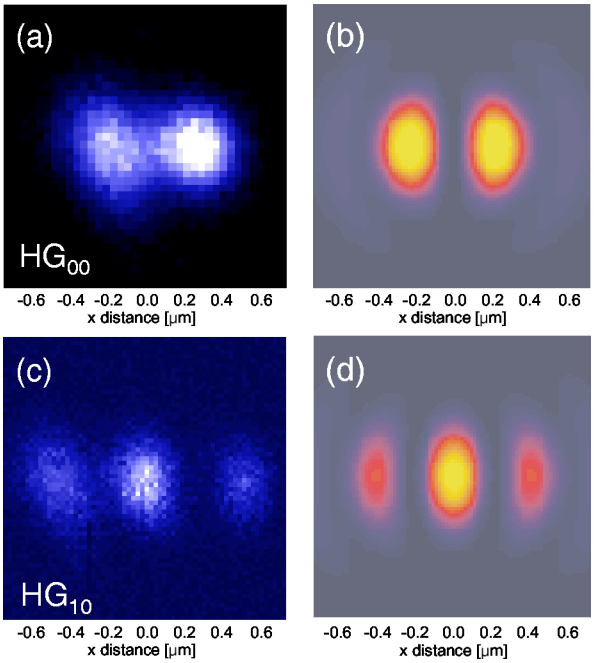

FIG. 9. Photoluminescence maps recorded by raster scanning a gold tip through tightly focused (a) HG_{00} and (c) HG_{10} beams. The recorded patterns correspond well with calculated longitudinal field distributions in (b) the HG_{00} focus and (d) the HG_{10} focus.

a combination of quasistatic lightning rod effect and localized surface plasmon resonances. The former effect arises from the singularity of electromagnetic fields at sharp edges or tips whereas surface plasmons resonances are modes of collective charge oscillations. Based on the typical dimensions of our gold tips we conclude that a field confinement to distances of 5–30 nm is required for efficient infrared photoluminescence generation. We have found that strong field enhancement is accompanied by strong infrared photoluminescence and we believe that infrared photoluminescence is therefore an indirect measure for the field enhancement at a particular gold nanostructure.

The field enhancement at a gold tip depends critically on the tip orientation with respect to the electric field polarization of the excitation beam.[24] To prove that the same polarization conditions are responsible for the generation of photoluminescence we took advantage of the inhomogeneous polarization in strongly focused laser beams.[25,26] As shown in Fig. 2, the tip can be raster scanned through the tightly focused laser beam while recording the photoluminescence intensity for every tip position. Figures 9(a) and 9(c) show the measured photoluminescence maps for a tightly focused Gaussian beam and a Hermite-Gaussian (HG_{10}) beam. We found that photoluminescence is predominantly observed when the electric field is polarized along the tip axis. The two-lobe pattern seen in Fig. 9(a) corresponds to the longitudinal field distribution in the focus of a Gaussian beam,[24,27] which is calculated in Fig. 9(b). Likewise, the three lobes in Fig. 9(c) represent the distribution of longitudinal fields in a focused HG_{10} mode.

Thus, we find that the tip only shows field enhancement and photoluminescence when it is excited along its axis. This means that the surface plasmon resonances correspond to longitudinal oscillations along the tip axis. Unlike an elliptical particle though, there is no boundary to set the resonance condition, which suggests that the optical response of the tip is due to the interaction of multiple plasmon quasimodes.

VII. CONCLUSIONS

We have measured the photoluminescence originating from smooth gold interfaces, particles, rough films, and sharp tips. We attribute the visible photoluminescence to interband recombination of holes in the *d* band with electrons in the conduction band near the Fermi surface. This signal can be excited directly with violet light, or with two-photon absorption in the near infrared. The spectrum of the photoluminescence represents the convolution of the electronic joint density of states between the two bands and the optical coupling efficiency due to the particular structure geometry and associated resonances. This coupling can be readily seen in the spectra obtained from individual gold particles.

For rough films, we observe both visible photoluminescence and a broad infrared signal. The infrared photoluminescence is linearly dependent on the near-infrared excitation power, and is excited with equal efficiency for both cw and femtosecond excitation. The signal is steady in time and does not bleach over the course of several hours. As long as some surface roughness remained, annealing of the films did not cause the signal to disappear. Photoluminescence from a gold tip shows the same power dependence and similar spectral features as those of a rough film. The polarization dependence of the tip photoluminescence showed a very strong enhancement for excitation fields polarized along the tip axis. We attribute the origin of the infrared signal to near-field optical intraband transitions which are coupled to the far field by the radiative decay of localized surface plasmons. We determined that the photoluminescence is confined to the near-field of a gold tip indicating that the critical size range to observe infrared emission from nanostructures is 5–30 nm.

ACKNOWLEDGMENTS

The authors would like to thank Achim Hartschuh, Jean-Jacques Greffet, and Tony Heinz for valuable discussions and suggestions. They also thank Brian McIntyre for assistance with SEM imaging, and Zheming Wang and Alan Joly for help with time-resolved measurements, which were performed in the Environmental Molecular Sciences Laboratory, a national user facility sponsored by the Department of Energy's Office of Biological and Environmental Research and located at Pacific Northwest National Laboratory. This work was funded by the U.S. Department of Energy through Grant No. DE-FG02-01ER15204 and partially supported by the Swiss Science National Foundation (A.B.).

*Electronic address: novotny@optics.rochester.edu

[1] A. Mooradian, Phys. Rev. Lett. **22**, 185 (1969).
[2] A. Otto, Surf. Sci. **85**, L392 (1978).
[3] R.L. Birke, J.R. Lombardi, and J.I. Gersten, Phys. Rev. Lett. **43**, 71 (1979).
[4] E. Burstein, Y.J. Chen, C.Y. Chen, S. Lundquist, and E. Tossati, Solid State Commun. **29**, 567 (1979).
[5] J.P. Heritage, J.G. Bergman, A. Pinczuk, and J.M. Worlock, Chem. Phys. Lett. **67**, 229 (1979).
[6] W. Steinmann, Phys. Solid State **28**, 437 (1968).
[7] J.C. Tsang, J.R. Kirtley, and T.N. Theis, Solid State Commun. **35**, 667l (1980).
[8] G.T. Boyd, Z.H. Yu, and Y.R. Shen, Phys. Rev. B **33**, 7923 (1986).
[9] V.A. Markel, V.M. Shalaev, P. Zhang, W. Huynh, L. Tay, T.L. Haslett, and M. Moskovits, Phys. Rev. B **59**, 10 903 (1999).
[10] J.P. Wilcoxon, J.E. Martin, F. Parsapour, B. Wiedenman, and D.F. Kelley, J. Chem. Phys. **108**, 9137 (1998).
[11] M.B. Mohamed, V. Volkov, S. Link, and M.A. El-Sayed, Chem. Phys. Lett. **317**, 517 (2000).
[12] O.P. Varnavski, M.B. Mohammed, M.A. El-Sayed, and T. Goodsen III, J. Phys. Chem. B **107**, 3101 (2003).
[13] C. Sönnichsen, T. Franzl, T. Wilk, G. von Plessen, J. Feldmann, O. Wilson, and P. Mulvaney, Phys. Rev. Lett. **88**, 077402 (2002).
[14] P.Y. Yu and M. Cardona, *Fundamentals of Semiconductors* (Springer-Verlag, Berlin, 1999), Chap. 6.
[15] E.J. Sánchez, L. Novotny, and X.S. Xie, Phys. Rev. Lett. **82**, 4014 (1999).
[16] A. Hartschuh, E.J. Sánchez, X.S. Xie, and L. Novotny, Phys. Rev. Lett. **90**, 095503 (2003).
[17] V.M. Shalaev, C. Douketis, T. Haslett, T. Stuckless, and M. Moskovits, Phys. Rev. B **53**, 11 193 (1996).
[18] M. Guerri and R. Rossei, Phys. Rev. B **12**, 557 (1975).
[19] R. Lässer, N.V. Smith, and R.L. Benbow, Phys. Rev. B **24**, 1895 (1980).
[20] D.J. Roaf, Philos. Trans. R. Soc. London **255**, 135 (1962).
[21] P.B. Johnson and R.W. Christy, Phys. Rev. B **6**, 4370 (1972).
[22] J.R. Zurita-Sánchez and L. Novotny, J. Opt. Soc. Am. B **19**, 1355 (2002).
[23] L. Libioulle, Y. Houbion, and J.-M. Gilles, J. Vac. Sci. Technol. B **13**, 1325 (1995).
[24] A. Bouhelier, M. Beversluis, A. Hartschuh, and L. Novotny, Phys. Rev. Lett. **90**, 013903 (2003).
[25] B. Sick, B. Hecht, and L. Novotny, Phys. Rev. Lett. **85**, 4482 (2000).
[26] L. Novotny, M.R. Beversluis, K.S. Youngworth, and T.G. Brown, Phys. Rev. Lett. **86**, 5251 (2001).
[27] L. Novotny, R.X. Bian, and X.S. Xie, Phys. Rev. Lett. **79**, 645 (1997).
[28] K. Karrai and R.D. Grober, Appl. Phys. Lett. **66**, 1842 (1995).
[29] P. Apell, R. Monreal, and S. Lundqvist, Phys. Scr. **38**, 174 (1987).
[30] G. Mie, Ann. Phys. (Leipzig) **25**, 377 (1908).
[31] R. Gans, Ann. Phys. (Leipzig) **47**, 270 (1915).
[32] S. Nie and S.R. Emory, Science **275**, 1102 (1997).
[33] K. Kneipp, Y. Wang, H. Kneipp, L.T. Perelman, I. Itzkan, R.R. Dasari, and M.S. Feld, Phys. Rev. Lett. **78**, 1667 (1997).
[34] A.M. Michaels, J. Jiang, and L. Brus, J. Phys. Chem. **104**, 11 965 (2000).
[35] C.F. Bohren and D.R. Huffman, *Absorption and Scattering of Light by Small Particles* (Wiley, New York, 1998).
[36] S. Link, A. Beeby, S. FitzGerald, M.A. El-Sayed, T.G. Schaff, and R.L. Whetten, J. Phys. Chem. B **106**, 3410 (2002).
[37] U. Kreibig, J. Phys. F: Met. Phys. **4**, 999 (1974).
[38] I. Campillo, A. Rubio, J.M. Pitarke, A. Goldmann, and P.M. Echenique, Phys. Rev. Lett. **85**, 3241 (2000).
[39] I. Campillo, J.M. Pitarke, A. Rubio, and P.M. Echenique, Phys. Rev. B **62**, 1500 (2000).
[40] J. Cao, Y. Gao, H.E. Elsayed-Ali, R.J.D. Miller, and D.A. Mantell, Phys. Rev. B **58**, 10 948 (1998).